Revista Mexicana de Astronomía y Astrofísica, **41**, 101–108 (2005)

THE EMISSION FROM PHOTOIONIZED STELLAR WIND BOW SHOCKS

J. Cantó,[1] A. C. Raga,[2] and R. F. González[2]

Received 2004 September 27; accepted 2005 January 19

RESUMEN

Choques a proa de vientos estelares fotoionizados aparecen en distintos objetos astrofísicos: regiones H II compactas, regiones H II alrededor de estrellas O desbocadas y choques a proa alrededor de estrellas jóvenes de baja masa dentro de regiones H II. Presentamos una formulación para calcular la medida de emisión a partir de modelos analíticos de capa delgada de choques a proa asociados a vientos estelares, con la cual se pueden hacer predicciones sencillas de la emisión de líneas de recombinación o del continuo libre-libre. Ilustramos el tipo de predicciones que pueden ser hechas calculando los mapas de emisión que resultan de un modelo de un choque a proa no-axisimétrico de un viento estelar.

ABSTRACT

Photoionized stellar wind bow shocks are found in a number of different astrophysical objects : compact H II regions, H II regions around runaway O stars and bow shocks around young, low mass stars within photoionized regions. We present a formulation for calculating the emission measure from analytic, thin shell stellar wind bow shock models, with which simple predictions of the recombination line or the free-free emission can be made. We illustrate the predictions that can be made by calculating the emission maps that result from a model of a non-axisymmetric stellar wind bow shock.

Key Words: **ISM: HERBIG-HARO OBJECTS – ISM: JETS AND OUTFLOWS – ISM: KINEMATICS AND DYNAMICS**

1. INTRODUCTION

A wind from a star in relative motion with respect to the surrounding environment produces a stellar wind bow shock. Such bow shocks are found in compact H II regions (in which the star is moving with respect to the surrounding molecular cloud, see, e.g., van Buren et al. 1990), and within H II regions around runaway O stars (in which the star is passing through the galactic plane, see, e.g., Noriega-Crespo, van Buren, & Dgani 1997). Also, the recently discovered "LL Ori objects" (Bally, O'Dell, & McCaughrean 2000; Bally & Reipurth 2001) are T Tauri stars with winds which interact with the expanding Orion Nebula (M42).

Van Buren et al. (1990) presented an analytic model for the region close to the stagnation point of a stellar wind bow shock. Mac Low et al. (1991) computed the "thin shell" bow shock numerically, and calculated the emission measure as a function of position in order to obtain predictions of free-free radio continuum maps. Stellar wind bow shocks have also been studied with full gasdynamical models (see, e.g., Dgani, van Buren, & Noriega-Crespo 1996; Raga et al. 1997).

The thin shell solution for stellar wind bow shocks was first obtained numerically by Baranov, Krasnobaev, & Kulikovskii (1971), and an analytic solution was found by Dyson (1975) in the "ram pressure balance" approximation (i.e., neglecting the centrifugal pressure term). Somewhat surprisingly, a full analytic solution to the thin shell, axisymmetric stellar wind bow shock was found by Wilkin (1996) and Cantó, Raga, & Wilkin (1996). Wilkin (2000) extended this work, obtaining full analytic solutions for non-axisymmetric stellar wind bow shocks.

In the present paper, we discuss a model for the stellar wind bow shocks in the LL Ori objects. While some of these objects show a prominent jet system, which probably dominates the interaction with the expanding Orion nebula, others appear to be the re-

[1]Instituto de Astronomía, Universidad Nacional Autónoma de México, México, D. F., México.

[2]Instituto de Ciencias Nucleares, Universidad Nacional Autónoma de México, México, D. F., México.

sult of the presence of a more or less isotropic stellar wind.

In these objects, both the stellar wind and the external shocks are radiative, so that the thin shell approach is directly applicable (its application to the case of O star bow shocks being somewhat more dubious because the stellar wind shock is non-radiative, see, e.g., Mac Low et al. 1991). With the exact solutions of Wilkin (1996; 2000) in mind, we calculate a density stratification (within the thin shell) which is consistent with the ram+centrifugal pressure balance, and then use this result to calculate the emission measure of the shell (§2). We then use this recipe for the emission measure in order to calculate emission maps (see §3) from one of the non-axisymmetric stellar wind bow shock solutions of Wilkin (2000). We finally present a discussion of the applicability of these models to the LL Ori objects in M42 (§4).

2. THE EMISSION MEASURE OF A THIN SHELL

2.1. *The Emission Measure in Terms of the Surface Density*

Let us consider the thin shell flow formed by a stellar wind and a surrounding environment which is flowing past the position of the star. This flow is shown in a schematic way in Figure 1. We assume that the stellar wind moves radially away from the star, and that the ambient flow moves in a fixed direction (e.g., we do not allow for a diverging or converging ambient flow). However, we do allow for the possibility of having an inhomogeneous ambient medium (i.e., with non-uniform density and/or velocity modulus) and/or a latitude-dependent stellar wind.

In this figure, we see the wind from a star (with a mass loss rate $\dot{M}_w$ and a radially constant wind velocity v_w) interacting with an environment of density ρ_a, which is flowing at a velocity v_a with respect to the star. The flow within the thin shell (which is limited by an inner, "stellar wind shock" and an outer "ambient shock" has a surface mass density σ, and is flowing along the shell at a velocity v.

We define a coordinate l measured inwards from the "ambient shock" (perpendicularly to the thin shell, see Fig. 1), so that the ambient shock is located at $l = 0$, and the stellar wind shock at $l = h$ (where h is the position-dependent thickness of the thin shell). Assuming that the flow within the shell is well mixed, it will be then flowing along the shell at a velocity v which is independent of l.

We now assume (as appropriate for the LL Ori objects) that the whole flow is photoionized by an external source, so that it can be approximated as an isothermal flow (at a temperature $T \approx 10^4$ K). Then, the pressure within the thin shell just behind the ambient shock will be

$$P_a = P(l = 0) = \rho_a {v_{a,n}}^2 \,, \qquad (1)$$

where ρ_a is the density of the ambient medium and $v_{a,n}$ the component of the ambient velocity normal to the thin shell, and the pressure just behind the stellar wind shock is

$$P_w = P(l = h) = \rho_w {v_{w,n}}^2 \,, \qquad (2)$$

where ρ_w is the density and $v_{w,n}$ the normal component of the stellar wind velocity (see Fig. 1). The pressure as a function of position l across the width

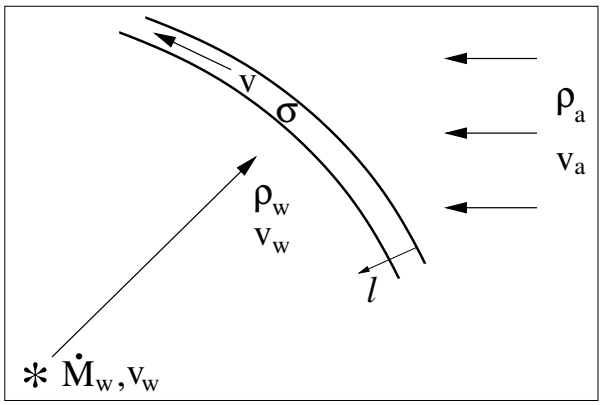

Fig. 1. Schematic diagram showing the thin shell flow resulting from the interaction of a stellar wind (of velocity v_w and mass loss rate $\dot{M}_w$) with an impinging ambient flow (of velocity v_a and density ρ_a). The thin shell is limited by a stellar wind shock and an ambient shock. The gas flows along the thin shell at a velocity v, and has a surface density σ. The coordinate l is measured inwards from the ambient shock, normal to the locus of the thin shell.

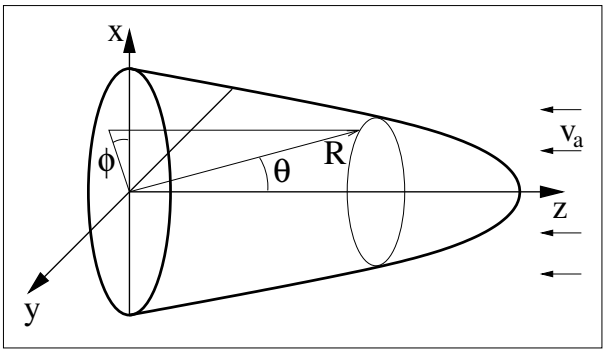

Fig. 2. Schematic diagram of a stellar wind bow shock, showing the definition of the spherical coordinate system used in §2 and §3.

of the thin shell is then described by the hydrostatic equation

$$\frac{dP}{dl} = -\rho\, g\,, \tag{3}$$

where $P = \rho c^2$ (with c being the isothermal sound speed) and the centrifugal acceleration being $g = v^2/R_c$ (where R_c is the radius of curvature of the curved flow streamlines). Equation (3) can be integrated with the boundary condition (1) to obtain:

$$P(l) = \rho(l)c^2 = P_a\, e^{-l/H}\,, \tag{4}$$

where $H \equiv c^2/g$ is the pressure (or density) scale height. The boundary condition on the stellar wind shock boundary (Eq. 2) then gives a relation between H and the width h of the thin shell

$$P_w = P_a\, e^{-h/H}\,, \tag{5}$$

using Eq. (4). Using Eqs. (4) and (5) we can now calculate the surface density

$$\sigma = \int_0^h \rho(l) dl = \frac{H}{c^2}\left(P_a - P_w\right)\,, \tag{6}$$

and the emission measure

$$EM = \int_0^h \left(\rho/\overline{m}\right)^2 dl = \frac{\left(P_a + P_w\right)\sigma}{2\overline{m}^2 c^2}\,, \tag{7}$$

where $\overline{m} \approx 1.4\, m_H$ is the average mass per hydrogen ion of the photoionized gas.

Let us now consider a spherical coordinate system (R, θ, ϕ), with the polar angle θ measured from the direction of the impinging ambient flow, as shown in Figure 2. The normal component of the pre-shock velocities (see Eqs. [1] and [2]) are then given by:

$$v_{a,n} = v_a \frac{\sin\theta[R\cos\theta + (\partial R/\partial\theta)\sin\theta]}{\sqrt{[R^2 + (\partial R/\partial\theta)^2]\sin^2\theta + (\partial R/\partial\phi)^2}}\,, \tag{8}$$

$$v_{w,n} = v_w \frac{R\sin\theta}{\sqrt{[R^2 + (\partial R/\partial\theta)^2]\sin^2\theta + (\partial R/\partial\phi)^2}}\,. \tag{9}$$

For the case of a uniform ambient medium and a spherically symmetric stellar wind, the flow would be axisymmetric, and therefore we would have $\partial R/\partial\phi = 0$, leading to much more simple equations for $v_{a,n}$ and $v_{w,n}$.

Combining Eqs. (1–2) and (8–9) we then obtain:

$$P_a = \rho_{a,0} {v_{a,0}}^2\, f_a(\theta,\phi)\,, \tag{10}$$

and

$$P_w = \rho_{a,0} {v_{a,0}}^2\, f_w(\theta,\phi)\,, \tag{11}$$

where

$$f_a(\theta,\phi) = \left(\frac{\rho_a v_a^2}{\rho_{a,0} v_{a,0}^2}\right) \times \frac{\sin^2\theta[R\cos\theta + (\partial R/\partial\theta)\sin\theta]^2}{[R^2 + (\partial R/\partial\theta)^2]\sin^2\theta + (\partial R/\partial\phi)^2}\,, \tag{12}$$

and

$$f_w(\theta,\phi) = \frac{R^2\sin^2\theta}{[R^2 + (\partial R/\partial\theta)^2]\sin^2\theta + (\partial R/\partial\phi)^2}\,, \tag{13}$$

where $\rho_{a,0}$ and $v_{a,0}$ are characteristic values of the ambient velocity and density (respectively), which we use to adimensionalize the equations.

2.2. *The Surface Density and the Flow Velocity*

With the results of §2.1, we can calculate the emission measure of the thin shell in terms of its surface density σ (see Eq. [7]). The remaining problem then is to calculate σ as a function of position on the thin shell.

In order to do this, we first note that the flow within the shell always follows trajectories with constant ϕ (see Fig. 2 and Wilkin 2000). The mass loss rate $\Delta\dot{M}$ flowing along a slice of angle $\Delta\phi$ of the thin shell is given by:

$$\Delta\dot{M} = (R\sin\theta) v \sigma\, \Delta\phi\,, \tag{14}$$

where R is the local radius of the thin shell, v the velocity along the thin shell, and σ its surface density. We then can find σ as a function of v:

$$\sigma = \frac{(d\dot{M}/d\phi)}{v\, R\sin\theta}\,, \tag{15}$$

where

$$\frac{d\dot{M}}{d\phi} \equiv \frac{\dot{M}_w}{4\pi} f_m(\theta,\phi)\,, \tag{16}$$

is the mass fed into the slice by the stellar wind and by the impinging ambient medium. An example of how to calculate $f_m(\theta,\phi)$ for a given model is shown in §3.

Now, in a completely equivalent way we can consider the z-momentum and the r-momentum (where r is the direction of the cylindrical radius) in order to obtain:

$$v_z = v_w \frac{f_z(\theta,\phi)}{f_m(\theta,\phi)}\,, \tag{17}$$

$$v_r = v_w \frac{f_r(\theta,\phi)}{f_m(\theta,\phi)}\,, \tag{18}$$

and the total velocity $v = \sqrt{v_z^2 + v_r^2}$ along the thin shell

$$v = v_w \frac{\sqrt{[f_z(\theta,\phi)]^2 + [f_r(\theta,\phi)]^2}}{f_m(\theta,\phi)}\,, \tag{19}$$

where $f_z(\theta,\phi)$ and $f_r(\theta,\phi)$ are intrinsic properties of the stellar wind+impinging ambient medium model defined through the relations:

$$\frac{d\dot{\Pi}_z}{d\phi} \equiv \frac{\dot{M}_w v_w}{4\pi} f_z(\theta,\phi)\,, \tag{20}$$

$$\frac{d\dot{\Pi}_r}{d\phi} \equiv \frac{\dot{M}_w v_w}{4\pi} f_r(\theta,\phi)\,, \tag{21}$$

where $d\dot{\Pi}_z/d\phi$ and $d\dot{\Pi}_r/d\phi$ are z- and r-momentum rates (respectively) inserted by the wind+impinging environment into the thin shell slice which we are considering.

Equation (19) can now be inserted into (15) in order to obtain the surface density as a function of position on the thin shell

$$\sigma(\theta,\phi) = \sigma_0\, f_\sigma(\theta,\phi)\,, \tag{22}$$

where

$$f_\sigma(\theta,\phi) = \frac{[f_m(\theta,\phi)]^2}{(R/R_0)\sin\theta\sqrt{[f_r(\theta,\phi)]^2+[f_z(\theta,\phi)]^2}} \tag{23}$$

is the function describing the angular dependence of σ,

$$\sigma_0 = \frac{v_a}{v_w}\left(\frac{\dot{M}_w\rho_0}{4\pi v_w}\right)^{1/2} \tag{24}$$

is the characteristic surface density, and

$$R_0 = \left(\frac{\dot{M}_w v_w}{4\pi\rho_{a,0}v_{a,0}^2}\right)^{1/2} \tag{25}$$

is the stagnation radius of the thin shell bow shock.

Finally, now that we have an expression for σ (Eq. [22]), we can combine it with Eq. (7) in order to obtain the emission measure of the shell as a function of position:

$$EM(\theta,\phi) = EM_0\,[f_a(\theta,\phi)+f_w(\theta,\phi)]\;f_\sigma(\theta,\phi)\,, \tag{26}$$

where

$$EM_0 = \frac{\rho_{a,0}v_{a,0}^2\sigma_0}{2\overline{m}^2c^2}\,. \tag{27}$$

We now finally have a calculation of the velocity along the thin shell v and the emission measure EM (Eqs. [19] and [26], respectively) given in terms of the functions f_a, f_w, f_m, f_r, f_z and $f_\sigma(\theta,\phi)$ (defined by Eqs. [12], [13], [16], [21], [20], and [23], respectively). In the following section, we calculate these functions for a specific stellar wind/impinging ambient medium model.

3. STELLAR WIND BOW SHOCK AGAINST A LINEARLY STRATIFIED AMBIENT MEDIUM

Let us now consider a stellar wind bow shock (see the schematic diagram of Fig. 2) of an isotropic stellar wind interacting with an impinging ambient medium of homogeneous velocity v_a, but with a stratified density of the form:

$$\rho_a = \rho_0 + a\,y\,, \tag{28}$$

where a is a constant (with dimensions of g cm^{-4}), and the y-axis is perpendicular to v_a (see Fig. 2). Wilkin (2000) found that the thin shell solution results in an equation for the spherical radius of the bow shock as a function of polar angle θ and azimuthal angle ϕ (see Fig. 2) of the form:

$$\frac{1}{3}R^2\sin^3\theta + \frac{\epsilon}{6}\sin\phi R^3\sin^4\theta + \theta\cos\theta - \sin\theta = 0\,, \tag{29}$$

where R is the spherical radius in units of R_0,

$$R_0 = \frac{1}{v_a}\sqrt{\frac{\dot{M}_w v_w}{4\pi\rho_0}}\,, \tag{30}$$

and

$$\epsilon \equiv \frac{aR_0}{\rho_0}\,. \tag{31}$$

Equation (29) can be inverted analytically or numerically to obtain $R(\theta,\phi)$.

For this solution, we can then calculate

$$f_a(\theta,\phi) = (1+\epsilon R\sin\phi\sin\theta)\times \frac{\sin^2\theta[R\cos\theta+(\partial R/\partial\theta)\sin\theta]^2}{[R^2+(\partial R/\partial\theta)^2]\sin^2\theta+(\partial R/\partial\phi)^2}\,, \tag{32}$$

and $f_w(\theta,\phi)$ which is given by Eq. (13) with the $R(\theta,\phi)$ calculated from Eq. (29). For this thin shell solution, Eq. (16) gives

$$\begin{aligned} f_m(\theta,\phi) &= 1-\cos\theta + \\ &+ \frac{v_w\sin^2\theta}{v_a}\left(\frac{1}{2}R^2+\frac{\epsilon}{3}R^3\sin\phi\sin\theta\right)\,, \end{aligned} \tag{33}$$

and Eq. (21) gives

$$f_r(\theta) = \frac{1}{2}\left(\theta-\sin\theta\cos\theta\right)\,. \tag{34}$$

This equation was previously derived by Cantó et al. (1996) and by Wilkin (2000). Finally, Eq. (20) gives

$$f_z(\theta,\phi) = \sin^2\theta\left(\frac{1-R^2}{2}-\frac{\epsilon}{3}R^3\sin\phi\sin\theta\right)\,, \tag{35}$$

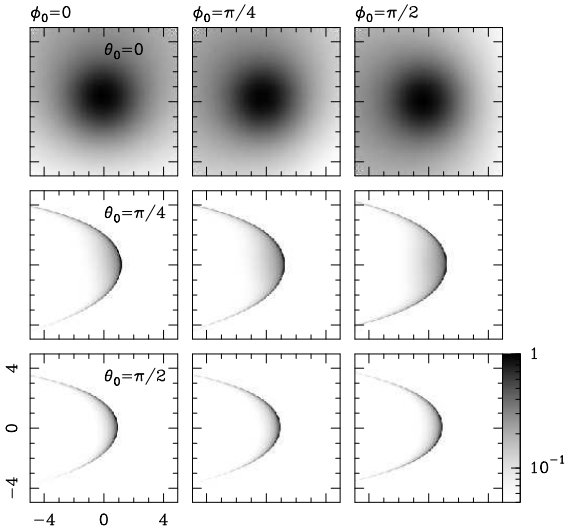

Fig. 3. Emission maps predicted from the $\epsilon = 0.1$ model, for different orientation of the flow with respect to the plane of the sky. The three columns correspond to line of sight directions with azimuthal angle $\phi = 0$, 45 and 90° (from left to right) and the three rows correspond to directions with polar angle $\theta = 0$, 45 and 90°. In the two bottom rows, the projection of the velocity v_a of the impinging ambient flow on the plane of the sky points from right to left along the abscissa. The axes are labeled in units of R_0 (see Eq. [30]). The maps are normalized with respect to the peak intensity value (within each of the maps), and are shown with the logarithmic greyscale given by the bar on the bottom right.

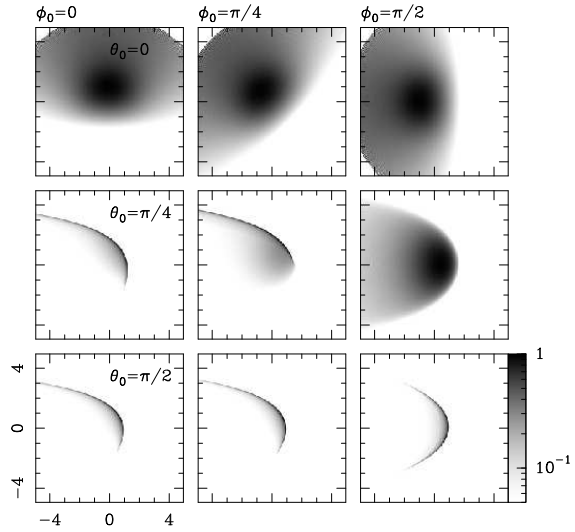

Fig. 4. Emission maps predicted from the $\epsilon = 0.5$ model, for different orientations of the flow with respect to the plane of the sky. The description of the graph is otherwise identical to the one of Fig. 3.

and $f_\sigma(\theta, \phi)$ is then given by Eq. (23).

With these results, Eqs. (19), (22), and (26) can be used to obtain the flow velocity v (along the thin shell), the surface density σ and the emission measure EM (respectively) as a function of position (θ, ϕ) on the thin shell bow shock.

The emission measure $EM(\theta, \phi)$ can be now used as an estimate of the H recombination line emission (or of the free-free continuum emission), and one can then carry out the appropriate line of sight integrations in order to obtain predicted emission maps from the thin shell model. This is done in the following section.

Finally, we note that the values for the "f_n" functions for $\theta = 0$ are:

$$f_a(\theta = 0) = \frac{16}{16 + \epsilon}\,, \tag{36}$$

$$f_w(\theta = 0) = \frac{16}{16 + \epsilon}\,, \tag{37}$$

$$f_m(\theta = 0) = 0\,, \tag{38}$$

$$f_r(\theta = 0) = 0\,, \tag{39}$$

$$f_z(\theta = 0) = 0\,, \tag{40}$$

$$f_\sigma(\theta = 0) = \frac{3\,(1 + v_w/v_a)^2}{\sqrt{16 + \epsilon^2 \sin^2\phi}}\,. \tag{41}$$

This last equation is nothing short of surprising. As can be seen from Eq. (22), Eq. (41) directly implies that at the stagnation point (i.e., at $\theta = 0$) the surface density (and hence the emission measure, see Eq. [26]) is multi-valued, as it has an explicit dependence on the azimuthal angle ϕ (see Eq. [41]).

This unphysical property of the solution is due to the fact that in the calculation of the transport of the material along the thin shell, the pressure of the gas has been neglected (see Eqs. [20] and [21]). The pressure of the gas (which is proportional to the surface density σ for an isothermal flow) guarantees that the properties of the flow are single valued and continuous through the stagnation point. However, in our zero-pressure model this desirable characteristic is not preserved.

We note that it is also possible to derive a purely "ram pressure balance" solution (in which the centrifugal pressure is neglected) for a stellar wind bow shock moving in a medium with a linearly stratified density. This ram pressure balance problem gives a solution of the form

$$R(\theta, \phi) = \frac{\left(1 + \frac{3}{2}\epsilon\theta\,\sin\phi\right)^{2/3} - 1}{\epsilon \sin\theta \sin\phi}\,, \tag{42}$$

which for $\epsilon = 0$ gives the well known solution of Dyson (1975) for the axisymmetric, ram pressure balance stellar wind bow shock. Using the ram pressure balance solution (Eq. [42]) instead of the full solution with centrifugal pressure (Eq. [29]) one can again determine the surface density of the thin shell. One then finds that the surface density of the ram pressure balance solution (Eq. [42]) has an behavior at $\theta = 0$ which is identical to the one of the solution with ram pressure balance, confirming the somewhat suspicious result of Eq. (41).

In the following section, we have computed models with $\epsilon = 0.1$ and 0.5 (see Eqs. [28] and [31]), and we find that the surface density σ and the emission measure EM are almost continuous through the stagnation point. For these values of ϵ, the jumps in σ and EM when going through the stagnation point have values of $< 2\%$ (as can be seen from Eq. [41]). Such small jumps do not produce important effects on the computed emission maps.

Clearly, if one considers models with larger values of ϵ, (so that the environmental density changes by factors of more than 2 over distances comparable to the stagnation radius of the bow shock) the jumps in σ and EM become larger. However, a linear approximation for the environmental density stratification (Eq. [28]) is meaningful only for small values of ϵ, i.e., for shallow stratifications that can be approximated with a linear spatial dependence. Therefore, for the particular problem that we are considering (of a wind/linearly stratified impinging environment interaction), the multivaluation of σ and EM for $\theta = 0$ does not introduce further limitations in the parameter range for which the model can be applied.

4. PREDICTED EMISSION MEASURE MAPS

We have computed the emission measure (see §2) for a pair of non-axisymmetric bow shock models. In order to compute the dimensionless shape (see Eq. [29]) and emission measure (Eq. [26]), it is necessary to specify two dimensionless parameters: ϵ (which gives the steepness of the stratification of the ambient medium, see Eqs. [28] and [31]) and the ratio v_w/v_a between the velocity of the stellar wind and the velocity of the impinging ambient medium. We have computed two models, with $v_w/v_a = 10$ (which is appropriate for a $v_w \sim 200$ km s^{-1} T Tauri wind interacting with a $v_a \sim 20$ km s^{-1} expanding H II region) and $\epsilon = 0.1$ and 0.5.

We have calculated the shape and the emission measure for these models, limiting the computed emission to the regions in which the density of the pre-bow shock ambient medium is positive (as can be seen from Eq.[28], for large enough values of y, $\rho_a < 0$). We then generate emission maps assuming that we observe the bow shock from an arbitrary direction (θ_0, ϕ_0) (where θ_0 is the polar angle and ϕ_0 the azimuthal angle of the lines of sight, see Fig. 2). The plane of the sky is of course perpendicular to this direction, and we describe it with a coordinate system so that its ordinate is parallel to the y-axis (i.e., the direction of the environmental density gradient) when $\phi_0 = 0$ and $\theta_0 = 0$.

Of course, as we have a model in which the thickness of the thin shell has been neglected, the predicted emission maps always have infinite intensity values in the regions where the thin shell is parallel to the lines of sight. We eliminate this problem by presenting maps which have been convolved with a square beam of $0.1\,R_0$ (where R_0 is the stagnation region radius of the bow shock, see Eq. [30]). This smoothing is meant to simulate the effect of the seeing in the maps of LL Ori objects (obtained by Bally et al. 2000) of angular sizes of a few arcseconds (with

TABLE 1

BOW SHOCK MODELS[a]

Map	ϵ	$\phi_0[^\circ]$	$\theta_0[^\circ]$	r[b]
S1	0.1	0	0	1.47
S2	0.1	0	45	1.22
S3	0.1	0	90	1.19
S4	0.1	45	0	1.31
S5	0.1	45	45	1.16
S6	0.1	45	90	1.13
S7	0.1	90	0	1.00
S8	0.1	90	45	1.00
S9	0.1	90	90	1.00
L1	0.5	0	0	6.37
L2	0.5	0	45	3.58
L3	0.5	0	90	3.23
L4	0.5	45	0	2.85
L5	0.5	45	45	2.39
L6	0.5	45	90	2.13
L7	0.5	90	0	1.00
L8	0.5	90	45	1.00
L9	0.5	90	90	1.00

[a]All of the models have have a ratio $v_w/v_a = 10$ between the velocity of the stellar wind and the velocity of the impinging ambient medium.

[b]r is the ratio between the emission measure integrated over the upper half and the lower half of the maps shown in Figures 3 and 4.

a seeing of a fraction of an arcsecond). Also, one could consider the effect of the actual width of the thin shell, but this width is much smaller than the seeing.

In this way, we have computed emission measure maps for 9 different lines of sight and for our two chosen $\epsilon = 0.1$, 0.5 values for the dimensionless density gradient (see Eq. [31]). The chosen values of (ϕ_0, θ_0) are listed in Table 1. Figure 3 shows the computed emission maps for the $\epsilon = 0.1$ model, and Figure 4 the ones for the $\epsilon = 0.5$ model.

These two figures illustrate the different morphologies that can be expected for non-axisymmetric, photoionized bow shocks. While the $\epsilon = 0.1$ model produces bow shocks that do not appear to have high asymmetries (see Fig. 3), the $\epsilon = 0.5$ model does produce clear asymmetries (see Fig. 4). In order to quantify the degree of asymmetry of the different maps, we have calculated the emission I_{top} integrated over the top half of the computed maps, and the emission I_{bot} integrated over the bottom half.

Table 1 gives the values of the $r = I_{top}/I_{bot}$ ratios obtained from all of the computed emission maps. For the maps of the $\epsilon = 0.1$ model we have $r \leq 1.5$, and for the maps of the $\epsilon = 0.5$ model we have larger asymmetries, with $r \leq 6.5$. The larger values of r are obtained for lines of sight with $\phi_0 = 0$ (for which the y-axis is parallel to the ordinate of the computed emission maps). For $\phi_0 = 90°$, we always have $r = 1$, which is natural since the projection of the y-axis on the plane of the sky is parallel to the abscissa.

5. CONCLUSIONS

In this paper, we have developed a model for calculating the emission measure from a thin shell flow solution. In this model, we assume that the flow within the thin shell is well mixed (so that there is a single value for the velocity as a function of position across the width of the thin shell), but we allow for a density stratification within the shell, which is formed as a result of the centrifugal pressure. This model is consistent with "full" thin shell calculations, in which the ram pressures of the flows (impinging on both sides of the thin shell) and the centrifugal pressure are considered.

In order to illustrate the possible applications of this model, we have applied it to the thin shell solution of Wilkin (2000) for a stellar wind interacting with an impinging ambient flow with a density gradient. We have then used the computed emission measure in order to obtain predicted emission maps for two different values of the dimensionless density gradient, $\epsilon = 0.1$ and 0.5, and different orientations of the flow with respect to the plane of the sky (see Eq. [31], Table 1, and Figs. 4 and 5).

The predicted maps can be compared directly with hydrogen recombination line maps of externally photoionized stellar wind bow shocks such as the ones found in the LL Orionis objects. From the papers of Bally et al. (2000) and Bally & Reipurth (2001), we see that the Hα maps of the LL Ori objects show limb-brightened, arc-like structures, with their "heads" pointing in the direction of θ Orionis (the photoionizing source of M 42). These objects do not have fully symmetric structures with respect to the axis pointing to θ Orionis. As we show in the present paper, such side-to-side asymmetries might be the result of large-scale density inhomogenieties in the density of the expanding H II region.

It is also possible that the observed asymmetries of the LL Ori objects might be the result of anisotropic, latitude-dependent winds being ejected by the associated T Tauri stars. From the observed emission maps, it is not possible to distinguish between asymmetries caused by an angular dependence of the stellar wind and asymmetries resulting from inhomogenieties in the expanding nebula. However, these two effects will lead to bow shocks with clearly different kinematical structures.

Therefore, it will be possible to use future high resolution spectro-imaging observations of LL Ori objects in order to deduce whether or not these objects show evidence for the presence of an angular dependence in the winds ejected from their associated T Tauri stars. As the formalism presented in §2 gives both the emission measure and the velocity along the thin shell, it can be used not only to obtain emission maps, but also to obtain predictions of spatially resolved line profiles, position-velocity diagrams and/or velocity channel maps. In this way, we already have a simple theoretical framework for interpreting spectro-imaging observations of LL Ori objects when they are made.

We end by noting a couple of limitations in our model. In the first place, our model is meant only for smooth environmental density stratifications, for which the assumption of a linear spatial dependence is a reasonable approximation. Secondly, we find that the thin shell formalism leads to a multivaluation of the surface density (and therefore the emission measure) of the thin shell at the stagnation point. While this is not a serious problem for our shallow environmental density stratification model, it might indeed be a problem in the case of other models for which this formalism could be applied,

and appropriate care should be taken in such future applications.

This work was supported by the CONACyT grants 36572-E, 41320-F, and 43103-F, and the DGAPA (UNAM) grants IN 112602 and IN 113605.

REFERENCES

Bally, J., O'Dell, C. R., & McCaughrean, M. J. 2000, AJ, 119, 2919

Bally, J., & Reipurth, B. 2001, ApJ, 546, 299

Baranov, V. B., Krasnobaev, K. V., & Kulikovskii, A. G. 1971, AovPhyD, 15, 791

Cantó, J., Raga, A. C., & Wilkin, F. 1996, ApJ, 469, 729

Dgani, R., van Buren, D., & Noriega-Crespo, A. 1996, ApJ, 461, 927

Dyson, J. E. 1975, Ap&SS, 35, 299

Raga, A. C., Noriega-Crespo, A., Cantó, J., Steffen, W., van Buren, D., Mellema, G., & Lundqvist, P. 1997, RevMexAA, 33, 73

Mac Low, M., Van Buren, D., Wood, D. O. S., & Churchwell, E. 1991, ApJ, 369, 395

Noriega-Crespo, A., Van Buren, D., & Dgani, R. 1997, AJ, 113, 780

van Buren, D., Mac Low, M., Wood, D. O. S., & Churchwell, E. 1990, ApJ, 353, 570

Wilkin, F. P. 1996, ApJ, 459, L31

_____. 2000, ApJ, 534, 400

Jorge Cantó: Instituto de Astronomía, UNAM, Apdo. Postal 70-264, 04510 México, D. F., México.

Ricardo González and Alejandro C. Raga: Instituto de Ciencias Nucleares, UNAM, Apdo. Postal 70-543, 04510 México, D. F., México (raga,ricardog@nuclecu.unam.mx).